Design and Experimental Validation of an H ∞ Observer for Vehicle Damper Force Estimation

Thanh-Phong Pham, Olivier Sename, Luc Dugard

Design and Experimental Validation of an $\mathcal{H}_\infty$ Observer for Vehicle Damper Force Estimation ⋆

Thanh-Phong Pham [*,**] **Olivier Sename** [*] **Luc Dugard** [*]

[*] *Univ. Grenoble Alpes, CNRS, Grenoble INP*[⊤]*, GIPSA-lab, 38000 Grenoble, France.* [⊤] *Institute of Engineering Univ. Grenoble Alpes (e-mail: thanh-phong.pham2, olivier.sename, luc.dugard@ gipsa-lab.grenoble-inp.fr).*

[**] *Faculty of Electrical and Electronic Engineering, University of Technology and Education, The University of Danang, 550000 Danang, Vietnam (e-mail: ptphong@ute.udn.vn)*

Abstract: The real-time estimation of damper force is crucial for control and diagnosis of suspension systems in road vehicles. In this study, we consider a semi-active electrorheological (ER) suspension system. First, a nonlinear quarter-car model is proposed that takes the nonlinear and dynamical characteristics of the semi-active damper into account. The estimation of the damper force is developed through a $\mathcal{H}_\infty$ observer whose objectives are to minimize the effects of bounded unknown road profile disturbances and measurement noises on the estimation errors of the state variables and nonlinearity through a Lipschitz assumption. The considered measured variables, used as inputs for the observer design, are the two accelerometers data from the sprung mass and the unsprung mass of the quarter-car system, respectively. Finally, the observer performances are assessed experimentally using the INOVE platform from GIPSA-lab (1/5-scaled real vehicle). Both simulation and experimental results emphasize the robustness of the estimation method against measurement noises and road disturbances, showing the effectiveness in the ability of estimating the damper force in real-time.

Keywords: Semi-active suspension, $\mathcal{H}_\infty$ observer, damping force estimation, Lipchitz condition,

1. INTRODUCTION

Nowadays, semi-active suspensions are widely used in vehicle applications due to their advantages compared to active and passive suspensions (Savaresi et al. (2010) and references therein). Central issues of these applications include dynamic modeling and control designs based on a reduced number of sensors to improve vehicle comfort and road holding. Depending on the characteristics of the adjustable shock absorber, models have been derived using several methodologies with different complexity and accuracy. Main models may be classified in terms of static and dynamic characteristics. Static models include Bingham model with Coulomb friction (see Stanway et al. (1987)), hysteresis based model (see Guo et al. (2006), de J Lozoya-Santos et al. (2012)). Dynamic models group considers the Bouc-Wen model in (Wen (1976), Ahmadian et al. (2004) and Spencer Jr et al. (1997)). Based on several approximators such as neural network (Chang and Roschke (1998), Chang and Zhou (2002)), fuzzy (Schurter and Roschke (2000)), polynomial (Du et al. (2005)) and among others (Savaresi et al. (2005)), proposed black box model can be also divided into static or dynamic groups, depending on the typical model. Generally, the common drawback of the above-mentioned dynamic models is the high complexity for controller and observer synthesis. Guo et al. (2006) introduced a semi-phenomenological model with high accuracy and control-oriented design. Noticeably, Guo's model only characterizes the static nonlinear behavior of semi-active suspensions. Therefore, how to extend the model taking into account both nonlinear and dynamic behaviors of the ER suspension system is needed.

Based on the above models, many control designs were proposed in the literature (see Poussot-Vassal et al. (2008), Priyandoko et al. (2009) and a review in Poussot-Vassal et al. (2012)). Some control design methodologies considered the damper force as the control input of the suspension system, then using an inverse model for implementation (see for instance Do et al. (2010), Nguyen et al. (2015)). Others use the force tracking control schemes in order to attain control objectives (Priyandoko et al. (2009)). Indeed, the damper force signal plays an important role in control synthesis. For this reason, several damper force estimation methodologies were presented (see Estrada-Vela et al. (2018), Reichhartinger et al. (2018), Tudon-Martinez et al. (2018), Koch et al. (2010), Rajamani and Hedrick (1995)), since in practice the damper force measurement is difficult and expensive. In (Koch et al. (2010)), parallel Kalman filters were developed to estimate the damper force without considering the dynamic behavior of the semi-active damper. Estrada-Vela

⋆ This work has been partially supported by the 911 scholarship from Vietnamese government. The authors also thank for financing project *EMPHYSIS*.

et al. (2018) introduced the H_∞ damping force observer using a dynamic nonlinear model of the ER damper, while requiring three sensors as inputs of observer. In order to reduce the number of the sensors and maintain a consideration of dynamic and nonlinear characteristics of MR damper, Tudon-Martinez et al. (2018) proposed a LPV-H_∞ filter to estimate the damper force using deflection and deflection velocity signals, which are difficult and expensive to measure in practice. Moreover, based on accelerometers, a full-car observer using the linearized model of the damper is proposed in (Dugard et al. (2012)) and gives interesting results both in simulations and experiments. Despite these achievements, the damping force observer based on the dynamic nonlinear model of semi-active ER suspension system and using low-cost sensors is still in demand.

To deal with the above problem, the H_∞ observer for Lipschitz nonlinear systems is a potential candidate since the nonlinear term in the ER model satisfies the Lipschitz condition. Over the years, many LMI-based observer designs for Lipschitz nonlinear systems were widely investigated in (Rajamani (1998), Zemouche and Boutayeb (2013), Pertew et al. (2006), Abbaszadeh and Marquez (2007), Darouach et al. (2011), Koenig (2006)). An interesting solution of designing observer for Lipschitz nonlinear system in the absence of unknown inputs was presented by (Phanomchoeng and Rajamani (2010)), based on the S-procedure lemma. Here, we aim to extend the approach to the Lipschitz system in the presence of sensor noises and unknown input disturbances and apply it to estimate the damping force of a semi-active suspension system.

In this paper, an $\mathcal{H}_\infty$ observer using two accelerometers is proposed in order to estimate the damper force in the presence of unknown road input and measurement noises. The design of the observer is based on a nonlinear suspension model consisting of a quarter-car vehicle model, augmented with a first order dynamical nonlinear damper model. Such a model captures the main behaviour of the ER dampers in an automotive applications. The major contribution of this paper are as follows:

- An H_∞ approach for Lipchitz nonlinear system is developed to design an observer minimizing, in an $\mathcal{L}_2$-induced gain objective, the effect of unknown inputs (road profile and measurement noises).
- The proposed observer has been implemented on a real scaled-vehicle test bench, through the Matlab/Simulink real-time workshop. The observer performances are then assessed with experimental tests

The remainder of this paper is organized as follows:

- Section 2: Semi-active suspension modeling.
- Section 3: Observer design.
- Section 4: Analysis of the observer design: frequency and time domains
- Section 5: Experimental validation
- Section 6: Conclusion

2. SEMI-ACTIVE SUSPENSION MODELING AND QUARTER-CAR SYSTEM DESCRIPTION

2.1 Semi-active suspension modeling

In the sequel, the dynamic nonlinear model for semi-active ER Damper is described. According to Guo et al. (2006), a phenomenological model of semi-active suspension can be represented by the following nonlinear equation:

$$F_d = k_0 x_d + c_0 \dot{x}_d + f_c.u.tanh(k_1 x_d + c_1 \dot{x}_d) \qquad (1)$$

where F_d is the damper force; c_0, c_1, k_0, k_1, f_c are constant parameters. $x_d, \dot{x}_d$ are deflection and deflection velocity of the damper, respectively. u is control input (in the available test bench, this is the duty cycle of the PWM signal that controls the application).

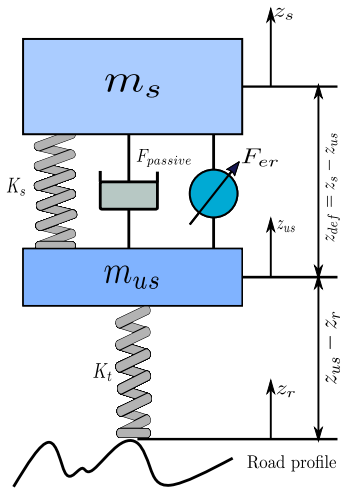

Fig. 1. 1/4 car model with semi-active suspension

From (1), the damper force F_d is separated into the passive and controlled parts as follows:

$$\begin{cases} F_d = k_0 x_d + c_0 \dot{x}_d + F_{nl}(x,u) \\ F_{nl}(x,u) = f_c.u.tanh(k_1 x_d + c_1 \dot{x}_d) \end{cases} \qquad (2)$$

Now in order to take into account the dynamical behavior of the ER fluid, it is important to complete the above model by including a first-order dynamical equation in the controlled part $F_{nl}(x,u)$:

$$\tau \dot{F}_{er} + F_{er} = F_{nl}(x,u) \qquad (3)$$

Therefore, the complete nonlinear damper dynamical model is given as

$$\begin{cases} F_d &= k_0 x_d + c_0 \dot{x}_d + F_{er} \\ \dot{F}_{er} &= -\dfrac{1}{\tau} F_{er} + \dfrac{f_c}{\tau} \Phi(x,u) \end{cases} \qquad (4)$$

where $\Phi(x,u) = u.tanh(k_1 x_d + c_1 \dot{x}_d)$

It is noted that linear and nonlinear indentification methodologies are used to determine all the parameters of the above model (shown in table 1). They are not described here since it is out of the scope of this paper.

2.2 Quarter-car system description

This section introduces the quarter-car model with the semi-active ER suspension system depicted in Fig.1. The well-known model consists of the sprung mass (m_s), the unsprung mass (m_{us}), the suspension components located between (m_s) and (m_{us}) and the tire which is modelled as a spring with stiffness k_t. From second law of Newton for motion, the system dynamics around the equilibrium are given as:

$$\begin{cases} m_s\ddot{z}_s & = -F_s - F_d \\ m_{us}\ddot{z}_{us} & = F_s + F_d - F_t \end{cases} \tag{5}$$

where $F_s = k_s(z_s - z_{us})$ is the spring force, $F_t = k_t(z_{us} - z_r)$ is the tire force, and the damper force F_d is given as in (4) with deflection $x_d = z_{def} = z_s - z_{us}$.

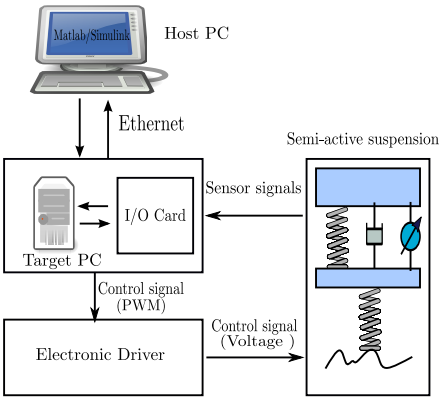

Fig. 2. Schematic diagram of testbed of semi-active suspension system

Subtituting (4) into (5), one easily obtains

$$\begin{cases} \ddot{z}_s & = -\dfrac{1}{m_s}\left[(k_s + k_0)(z_s - z_{us}) + c_0(\dot{z}_s - \dot{z}_{us}) + F_{er}\right] \\ \ddot{z}_{us} & = \dfrac{1}{m_{us}}[(k_s + k_0)(z_s - z_{us}) + c_0(\dot{z}_s - \dot{z}_{us}) + F_{er} \\ & \quad -k_t(z_{us} - z_r)] \\ \dot{F}_{er} & = -\dfrac{1}{\tau}F_{er} + \dfrac{f_c}{\tau}\Phi(x,u) \end{cases} \tag{6}$$

where z_s and z_{us} are the displacements of the sprung and unsprung masses, respectively; z_r is the road displacement input.

By selecting the system states as $x = [x_1, x_2, x_3, x_4, x_5]^T = [z_s - z_{us}, \dot{z}_s, z_{us} - z_r, \dot{z}_{us}, F_{er}]^T \in \mathbb{R}^5$ and the measured variables $y = [\ddot{z}_s, \ddot{z}_{us}]^T \in \mathbb{R}^2$, the system dynamics in the state-space representation can be written as follows

$$\begin{cases} \dot{x} & = Ax + B\Phi(x,u) + D_1\omega \\ y & = Cx + D_2\omega \end{cases} \tag{7}$$

where

$$A = \begin{bmatrix} 0 & 1 & 0 & -1 & 0 \\ -\dfrac{(k_s+k_0)}{m_s} & -\dfrac{c_0}{m_s} & 0 & \dfrac{c_0}{m_s} & -\dfrac{1}{m_s} \\ 0 & 0 & 0 & 1 & 0 \\ \dfrac{(k_s+k_0)}{m_{us}} & \dfrac{c_0}{m_{us}} & -\dfrac{k_t}{m_{us}} & -\dfrac{c_0}{m_{us}} & \dfrac{1}{m_{us}} \\ 0 & 0 & 0 & 0 & -\dfrac{1}{\tau} \end{bmatrix}$$

$$C = \begin{bmatrix} -\dfrac{(k_s+k_0)}{m_s} & -\dfrac{c_0}{m_s} & 0 & \dfrac{c_0}{m_s} & -\dfrac{1}{m_s} \\ \dfrac{(k_s+k_0)}{m_{us}} & \dfrac{c_0}{m_{us}} & -\dfrac{k_t}{m_{us}} & -\dfrac{c_0}{m_{us}} & \dfrac{1}{m_{us}} \end{bmatrix}$$

$$B = \begin{bmatrix} 0 \\ 0 \\ 0 \\ 0 \\ \dfrac{f_c}{\tau} \end{bmatrix}, D_1 = \begin{bmatrix} 0 & 0 \\ 0 & 0 \\ -1 & 0 \\ 0 & 0 \\ 0 & 0 \end{bmatrix}, D_2 = \begin{bmatrix} 0 & 0.01 \\ 0 & 0.01 \end{bmatrix}$$

$\omega = \begin{pmatrix} \dot{z}_r \\ n \end{pmatrix}$, in which, $\dot{z}_r$ is the road profile derivative and n is the sensor noises.

The control input function $\Phi(x,u)$ of the system (7) can be rewritten under the following form

$$\begin{aligned} \Phi(x,u) &= u.tanh\left([k_1 \ c_1 \ 0 \ -c_1 \ 0] \begin{bmatrix} x_1 \\ x_2 \\ x_3 \\ x_4 \\ x_5 \end{bmatrix} \right) \\ &= u.tanh(\Gamma x) \end{aligned} \tag{8}$$

where $\Gamma = [k_1,\ c_1,\ 0,\ -c_1,\ 0]$

Therefore, $\Phi(x,u)$ satisfies the Lipschitz condition in x

$$\|\Phi(x,u) - \Phi(\hat{x},u)\| \leqslant \|\Gamma(x - \hat{x})\|, \forall x, \hat{x} \tag{9}$$

Note that the measured outputs $y = [\ddot{z}_s, \ddot{z}_{us}]^T$ can be obtained easily from on board sensors (accelerometers).

Table 1. Parameter values of the quarter-car model equipped with an ER damper

Parameter	Description	value	Unit
m_s	Sprung mass	2.27	kg
m_{us}	unsprung mass	0.25	kg
k_s	Spring stiffness	1396	N/m
k_t	Tire stiffness	12270	N/m
k_0	Passive damper stiffness coefficient	170.4	N/m
c_0	Viscous damping coefficient	68.83	N.s/m
k_1	Hysteresis coefficient due to displacement	218.16	N.s/m
c_1	Hysteresis coefficient due to velocity	21	N.s/m
f_c	Dynamic yield force of ER fluid	28.07	N
τ	Time constant	43	ms

3. OBSERVER DESIGN

In this section, an H_∞ observer is developed to estimate the damping force accurately. The unknown input ω (road profile disturbance and measurement noise) is considered as an unknown disturbance. Therefore, an H_∞ observer is proposed to minimize the effect of the accounting for unknown disturbance ω on the state estimation errors and to bound the nonlinearity by Lipschitz constant.

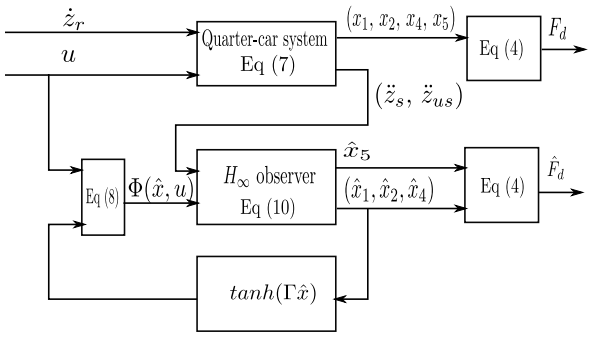

Fig. 3. Block diagram of the $\mathcal{H}_\infty$ damper force observer

3.1 $\mathcal{H}_\infty$ observer design

The H_∞ observer for the quarter-car system (7) is defined as follows

$$\dot{\hat{x}} = A\hat{x} + L(y - C\hat{x}) + B\Phi(\hat{x}, u) \tag{10}$$

where $\hat{x}$ is the estimated states. The observer gain L will be determined in the next steps

The estimation error is given as

$$e(t) = x(t) - \hat{x}(t) \tag{11}$$

Differentiating $e(t)$ with respect to time and using (7) and (10), one obtains

$$\begin{aligned}\dot{e} &= \dot{x} - \dot{\hat{x}} \\ &= Ax + B\Phi(x,u) + D_1\omega \\ &- A\hat{x} - L(y - C\hat{x}) - B\Phi(\hat{x},u) \\ &= (A - LC)e + B(\Phi(x,u) - \Phi(\hat{x},u)) + (D_1 - LD_2)\omega\end{aligned} \tag{12}$$

Assuming the Lipschitz condition (9) for $\Phi(x,u)$, the $\mathcal{H}_\infty$ observer design objective is stated below

- The system (12) is stable for $\omega(t) = 0$
- $\|e(t)\|_{\mathcal{L}_2} < \gamma\|\omega(t)\|_{\mathcal{L}_2}$ for $\omega(t) \neq 0$

The following theorem solves the above problem into an LMI framwork.

Theorem 1. Consider the system model (7) and the observer (10) . Given positive scalars γ and ϵ_l. The system (12) is asymptotically stable for $\omega = 0$ and $\frac{\|e(t)\|_{\mathcal{L}_2}}{\|\omega(t)\|_{\mathcal{L}_2}} < \gamma$ for $\omega(t) \neq 0$ if there exist a symmetric positive definite matrix P and a matrix Y satisfying

$$\begin{bmatrix} \Omega & PB & PD_1 + YD_2 \\ * & -\epsilon_l I_d & 0_{n,d} \\ * & * & -\gamma^2 I \end{bmatrix} < 0 \tag{13}$$

where $\Omega = A^TP + PA + YC + C^TY^T + \epsilon_l\Gamma^T\Gamma + I_n$

The observer matrix will be then $L = -P^{-1}Y$

Proof. Consider the following Lyapunov function

$$V(t) = e(t)^T P e(t) \tag{14}$$

Differentiating $V(t)$ along the solution of (12) yields

$$\begin{aligned}\dot{V}(t) &= \dot{e}(t)^T P e(t) + e(t)^T P \dot{e}(t) \\ &= [(A - LC)e + B(\Phi(x,u) - \Phi(\hat{x},u)) \\ &+ (D_1 - LD_2)\omega]^T P e + e^T P[(A - LC)e \\ &+ B(\Phi(x,u) - \Phi(\hat{x},u)) + (D_1 - LD_2)\omega] \\ &= \begin{bmatrix} e^T \\ (\Phi(x,u) - \Phi(\hat{x},u))^T \\ \omega^T \end{bmatrix}^T \times \\ &\begin{bmatrix} (A - LC)^TP + P(A - LC) & PB & P(D_1 - LD_2) \\ B^TP & 0 & 0 \\ (D_1 - LD_2)^TP & 0 & 0 \end{bmatrix} \\ &\times \begin{bmatrix} e \\ \Phi(x,u) - \Phi(\hat{x},u) \\ \omega \end{bmatrix}\end{aligned} \tag{15}$$

For brevity, define $\eta = \begin{bmatrix} e \\ \Phi(x,u) - \Phi(\hat{x},u) \\ \omega \end{bmatrix}$, then one obtains

$$\dot{V}(t) = \eta^T M \eta \tag{16}$$

where

$$M = \begin{bmatrix} \Omega_1 & PB & P(D_1 - LD_2) \\ B^TP & 0 & 0 \\ (D_1 - LD_2)^TP & 0 & 0 \end{bmatrix}$$

with $\Omega_1 = (A - LC)^TP + P(A - LC)$

From (9), the following condition is obtained

$$\begin{aligned}&(\Phi(x,u) - \Phi(\hat{x},u))^T(\Phi(x,u) - \Phi(\hat{x},u)) \leqslant e^T\Gamma^T\Gamma e \\ \Leftrightarrow &\begin{bmatrix} e^T \\ (\Phi(x,u) - \Phi(\hat{x},u))^T \end{bmatrix}^T \times \\ &\begin{bmatrix} -\Gamma^T\Gamma & 0 \\ 0 & I \end{bmatrix} \begin{bmatrix} e \\ (\Phi(x,u) - \Phi(\hat{x},u)) \end{bmatrix} \leqslant 0 \\ \Leftrightarrow &\eta^T Q \eta \leqslant 0\end{aligned} \tag{17}$$

where $Q = \begin{bmatrix} -\Gamma^T\Gamma & 0 & 0 \\ 0 & I & 0 \\ 0 & 0 & 0 \end{bmatrix}$

In order to satisfy the objective design w.r.t. the $\mathcal{L}_2$ gain disturbance attenuation, the $\mathcal{H}_\infty$ performance index is defined as:

$$\begin{aligned}J &= e^Te - \gamma^2\omega^T\omega \\ &= \begin{bmatrix} e^T \\ \omega^T \end{bmatrix}^T \begin{bmatrix} I & 0 \\ 0 & -\gamma^2 I \end{bmatrix} \begin{bmatrix} e \\ \omega \end{bmatrix} \\ &= \eta^T R \eta\end{aligned} \tag{18}$$

where $R = \begin{bmatrix} I & 0 & 0 \\ 0 & 0 & 0 \\ 0 & 0 & -\gamma^2 I \end{bmatrix}$

By applying the $\mathcal{S}$-procedure Boyd et al. (1994) to the two contraints (17) and $J \leqslant 0$, $\dot{V}(t) < 0$ if there exists a scalar $\epsilon_l > 0$ such that

$$\begin{aligned}&\dot{V}(t) - \epsilon_l(\eta^TQ\eta) + J < 0 \\ \Leftrightarrow &\eta^TM\eta - \epsilon_l(\eta^TQ\eta) + \eta^TR\eta < 0 \\ \Leftrightarrow &\eta^T(M - \epsilon_l Q + R)\eta < 0\end{aligned} \tag{19}$$

The condition (19) is equivalent to

$$M - \epsilon_l Q + R < 0$$
$$\Leftrightarrow \begin{bmatrix} \Omega_1 + \epsilon_l \Gamma^T \Gamma + I & PB & P(D_1 - LD_2) \\ B^T P & -\epsilon_l I & 0 \\ (D_1 - LD_2)^T P & 0 & -\gamma^2 I \end{bmatrix} < 0 \qquad (20)$$

Let define $Y = -PL$ and substitute into (20), the LMI (13) is obtained. □

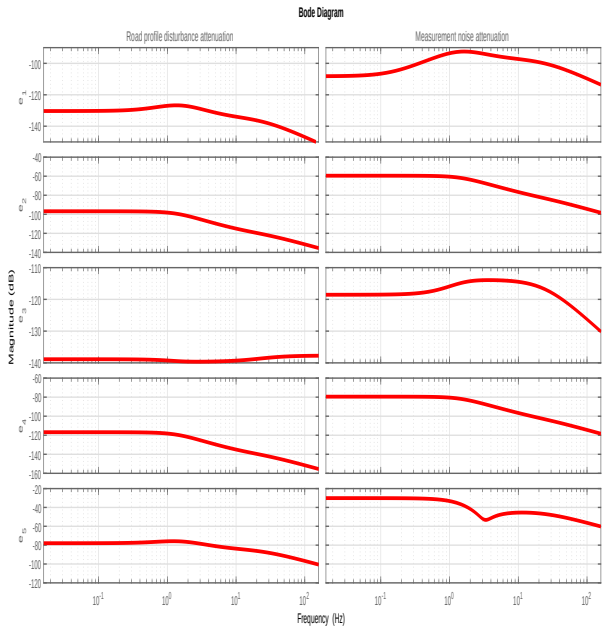

Fig. 4. Transfer $\|e/\omega\|$- Bode diagrams

4. ANALYSIS OF THE OBSERVER DESIGN: FREQUENCY AND TIME DOMAINS

In this section, the synthesis result of the $\mathcal{H}_\infty$ observer is presented and some simulation results are given.

4.1 Synthesis results and frequency domain analysis

Solving *theorem 1* with $\epsilon_l = 2$, we obtain the $\mathcal{L}_2$ gain $\gamma = 1.1938$ and the observer gain

$$L = \begin{bmatrix} -0.1947 & -0.0051 \\ -1.1537 & -0.0321 \\ -12.7490 & -167.4689 \\ -0.2154 & 0.9968 \\ -87.9502 & -1.4818 \end{bmatrix}$$

The resulting attenuation of the sensor noises and road profile disturbance on the estimation error, subject to the minimization problems, is shown in Figure 4. These results emphasize the attenuation level of measurement noises and unknown road profile effect on the 5 estimation errors, since the largest sensor noise and road profile disturbance amplification of the 5 errors, over the whole frequency range, are -30dB and -77dB, respectively.

4.2 Simulation

To demonstrate the effectiveness of the proposed design, the simulations are made with the nonlinear quarter-car model (7). The block-scheme given in Figure 3 illustrates how the simulations of the $\mathcal{H}_\infty$ observer are done. The following initial conditions of the proposed observer are considered:

$$x_0 = [0\ 0\ 0\ 0\ 0]^T$$
$$\hat{x}_0 = [0.01,\ -0.4,\ 0.001,\ -0.15,\ 2]^T$$

Two simulation scenarios are used to evaluate the performance of the observer as follows:

Scenario 1:

- The road profile is a sequence of sinusoidal bumps $z_r = 15sin(4\pi t)(mm)$.
- The duty cycle $u = 0.1$ is chosen

Scenario 2:

- An ISO 8608 road profile signal (Type C) is used.
- The duty cycle $u = 0.1$

The simulation results of two tests are shown in the Fig. 5 and Fig. 6. It can be clearly observed in Fig. 5 and Fig. 6 that the damping force is estimated with a satisfactory accuracy.

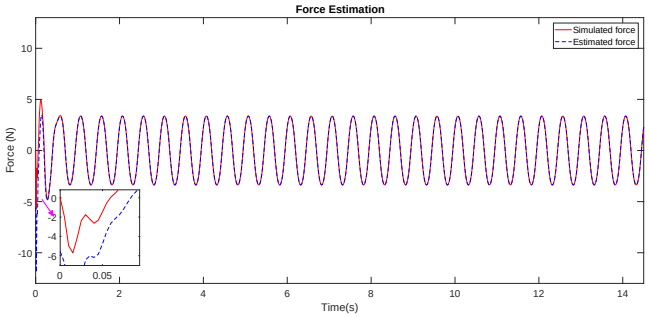

Fig. 5. Simulation scenario 1: Estimated force v.s real force

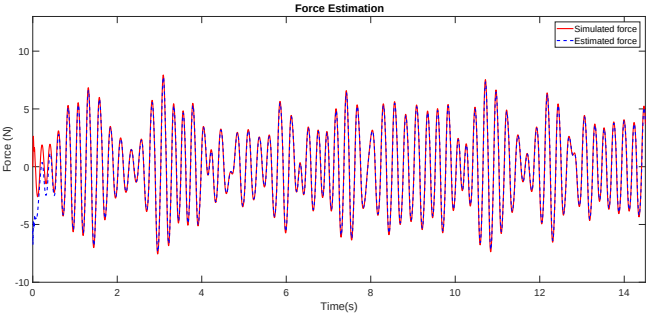

Fig. 6. Simulation scenario 2: Estimated force v.s real force

4.3 Robustness analysis

In this section, the μ-tool is used to analyse the robustness of the H_∞ observer. The estimation error dynamics (12), including the system model (7) and the observer (10), is analysed here.

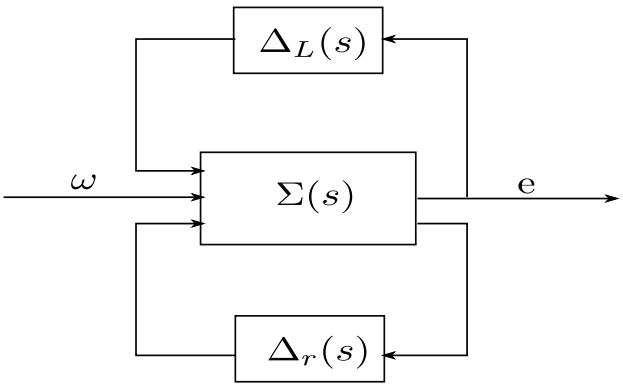

Fig. 7. Uncertain system for robust stability analysis

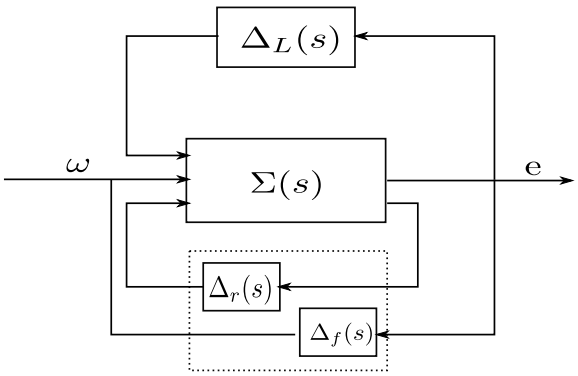

Fig. 8. Uncertain system for robust performance analysis

The two main types of uncertainties are the Lipschitz nonlinear matrix Γ and the time-varying parametric uncertainty, concerning the unsprung mass, the sprung mass, the spring stiffness and the damper model coefficients. In particular, the parametric uncertainties are shown in the Table 2 and a Lipschitz nonlinear uncertainty is assumed as follows

$$\Phi_\Delta(x,u) = \Phi(x,u) + \Delta\Phi(x,u) \tag{21}$$

where

$$\|\Delta\Phi(x,u) - \Delta\Phi(\hat{x},u)\| \leqslant \|\Delta\Gamma(x-\hat{x})\| \tag{22}$$

with $\Delta\Gamma = \Gamma_\Delta - \Gamma$

The estimation error dynamics (12) in the uncertain domain is rewritten as follows

$$\begin{aligned}\dot{e}_\Delta = (A_\Delta - LC_\Delta)e + B_\Delta(\Phi_\Delta(x,u) - \Phi_\Delta(\hat{x},u)) \\ + (D_{1\Delta} - LD_{2\Delta})\omega\end{aligned} \tag{23}$$

where A_Δ, B_Δ, C_Δ, $D_{1\Delta}$, $D_{2\Delta}$ are the system matrices considering the uncertainties.

The system (23) is written into the LFT representations (see Figure 7 and Figure 8). In which, $\Sigma(s)$ is the system (23) with nominal values of parameters, shown in the Table 2. $\Delta_r(s)$ represents the parametric uncertainties shown in the Table 2. $\Delta_L(s)$ is the uncertain Lipschitz condition (22). The performance objectives are represented by the fictitious uncertainties $\Delta_f(s)$.

Table 2. Parameter values of the quarter-car model equipped with an ER damper

Uncertain parameters	Variation
m_s	2.27 $\mp$ 50%(kg)
m_{us}	0.25$\mp$ 20%(kg)
k_s	1396$\mp$ 20%(N/m)
k_t	12270 $\mp$ 20%(N/m)
k_0	170.4$\mp$ 20%(N/m)
c_0	68.83$\mp$ 20%(N.s/m)
k_1	218.16$\mp$ 20%(N.s/m)
c_1	21$\mp$ 20%(N.s/m)
f_c	28.07$\mp$ 20%
τ	43$\mp$ 20%(ms)

Both robust stability and performance analysis are based on the LFT representations of the uncertain systems (shown in Figure 7 and Figure 8, respectively). These results are presented in the Fig.9, where the upper and lower bounds of μ are always less than 1. Therefore, the robust stability and robust performance of the observer system are guaranteed. Note that the observer is stable even for larger uncertainties.

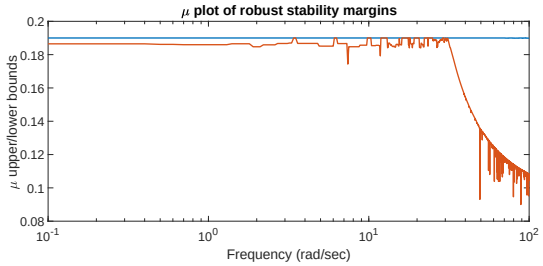

(a)

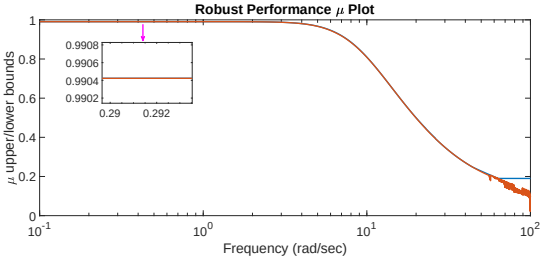

(b)

Fig. 9. (a) Robust stability analysis, (b) Robust performance analysis

5. EXPERIMENTAL VALIDATION

To validate the effectiveness of the proposed algorithm, experiments have been performed on the 1/5 car scaled car INOVE available at GIPSA-lab, shown in Fig. 10.

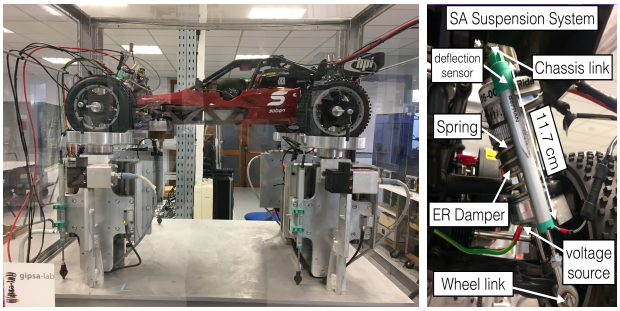

Fig. 10. The experimental testbed INOVE at GIPSA-lab (see www.gipsa-lab.fr/projet/inove)

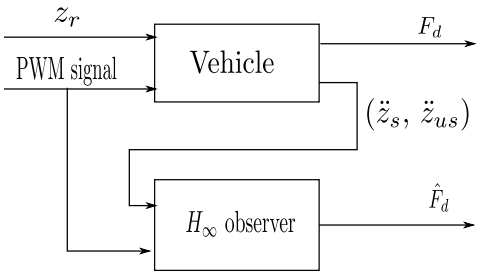

Fig. 11. Block diagram for implementation of the $\mathcal{H}_\infty$ damper force observer

Table 3. Normalized Root-Mean-Square Errors

Road Profile Sequence	Simulation	Experiment
Sinusoidal bumps	0.0234	0.0896
ISO 8608 road	0.0366	0.1015

This test-bench which involves 4 semi-active ER suspensions is controlled in real-time using xPC target and a host computer. The target PC is connected to the host computer via Ethernet communication standard (see Figure 2). The proposed observer system is implemented on the host PC using Matlab/simulink with the sampling time $T_s = 0.05s$. Note that the experimetal platform is fully equipped sensors to measure its vertical motion. Each corner of the system has a DC motor to generate the road profile.

In this study, the damping force estimation algorithm is applied for the rear-left corner whose available sensors are the unsprung mass accelerometer $\ddot{z}_{us}$, the sprung mass accelerometer $\ddot{z}_s$, the damping force sensor F_d, and the position sensors to measure suspension deflection z_{def}, road profile z_r and unsprung mass position z_{us}. As previously mentioned, only both unsprung mass acceleration $\ddot{z}_{us}$ and sprung mass acceleration $\ddot{z}_s$ are used as inputs of the proposed observer. The following block-scheme illustrates the experiment scenario of the observer (shown in Fig. 11)

In this experiment senario, the duty cycle of PWM signal is constant $u = 0.1$ and the real road profiles are sequence of sinusoidal bumps and ISO 8608 road, shown in Fig. 12(a) and Fig. 13(a), respectively. The experiment results of the observer are presented in Fig. 12 (b) and Fig. 13 (b). The result illustrates the accuracy and efficiency of the proposed observer. To further describe this accuracy, Table 3 presents the normalized root-mean-square errors, considering the difference between the estimated and measured forces, for the simulation and experimental results presented in the Fig. 5, Fig. 12 (b) and Fig. 13 (b).

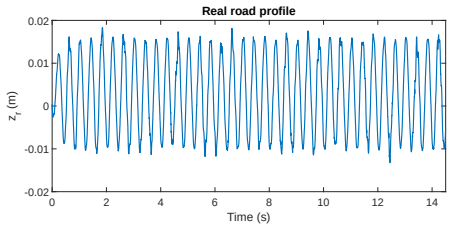

(a)

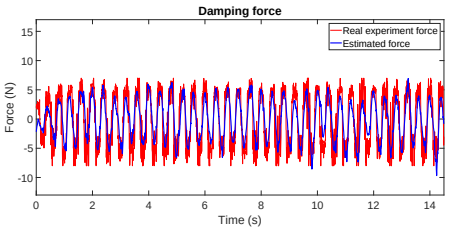

(b)

Fig. 12. Experiment test 1: (a) Road profile, (b) Real force vs. Estimated force

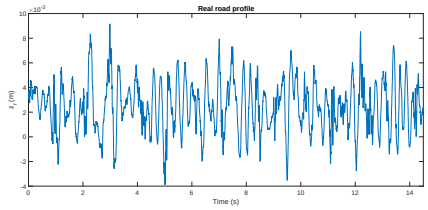

(a)

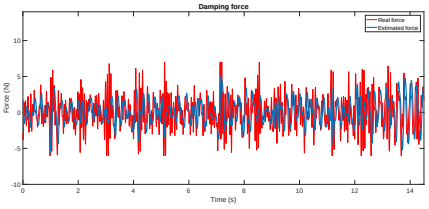

(b)

Fig. 13. Experiment test 2: (a) Road profile, (b) Real force vs. Estimated force

6. CONCLUSION

This paper presented an LMI-based $\mathcal{H}_\infty$ observer to estimate the damper force, based on the dynamic nonlinear model of the ER damper. For this purpose, the quarter-car system is represented by considering a phenomenological model of damper. Using two accelerometers, an $\mathcal{H}_\infty$ observer is designed, providing a good estimation result of the damping force. The estimation error is minimized accounting for the effect of unknown inputs (road profile disturbance and measurement noises) and the nonlinearity term bounded by a Lipchitz condition. The robust statbiliy and robust performance properties are ensured by using the μ tool. Both simulation and experiment results assess

the ability and the accuracy of the proposed models to estimate the damping force of the ER semi-active damper.

REFERENCES

Abbaszadeh, M. and Marquez, H.J. (2007). Robust h observer design for a class of nonlinear uncertain systems via convex optimization. In *American Control Conference, 2007. ACC'07*, 1699–1704. IEEE.

Ahmadian, M., Song, X., and Southward, S.C. (2004). No-jerk skyhook control methods for semiactive suspensions. *Transactions of the ASME-L-Journal of Vibration and Acoustics*, 126(4), 580.

Boyd, S., El Ghaoui, L., Feron, E., and Balakrishnan, V. (1994). *Linear matrix inequalities in system and control theory*, volume 15. Siam.

Chang, C.C. and Roschke, P. (1998). Neural network modeling of a magnetorheological damper. *Journal of intelligent material systems and structures*, 9(9), 755–764.

Chang, C.C. and Zhou, L. (2002). Neural network emulation of inverse dynamics for a magnetorheological damper. *Journal of Structural Engineering*, 128(2), 231–239.

Darouach, M., Boutat-Baddas, L., and Zerrougui, M. (2011). H observers design for a class of nonlinear singular systems. *Automatica*, 47(11), 2517–2525.

de J Lozoya-Santos, J., Morales-Menendez, R., Ramirez-Mendoza, R., Tudon-Martinez, J.C., Sename, O., and Dugard, L. (2012). Magnetorheological damperan experimental study. *Journal of Intelligent Material Systems and Structures*, 23(11), 1213–1232.

Do, A.L., Sename, O., and Dugard, L. (2010). An lpv control approach for semi-active suspension control with actuator constraints. In *American Control Conference (ACC), 2010*, 4653–4658. IEEE.

Du, H., Sze, K.Y., and Lam, J. (2005). Semi-active h control of vehicle suspension with magneto-rheological dampers. *Journal of Sound and Vibration*, 283(3), 981–996.

Dugard, L., Sename, O., Aubouet, S., and Talon, B. (2012). Full vertical car observer design methodology for suspension control applications. *Control Engineering Practice*, 20(9), 832–845.

Estrada-Vela, A., Alcántara, D.H., Menendez, R.M., Sename, O., and Dugard, L. (2018). H observer for damper force in a semi-active suspension. *IFAC-PapersOnLine*, 51(11), 764–769.

Guo, S., Yang, S., and Pan, C. (2006). Dynamic modeling of magnetorheological damper behaviors. *Journal of Intelligent material systems and structures*, 17(1), 3–14.

Koch, G., Kloiber, T., and Lohmann, B. (2010). Nonlinear and filter based estimation for vehicle suspension control. In *Decision and Control (CDC), 2010 49th IEEE Conference on*, 5592–5597. IEEE.

Koenig, D. (2006). Observers design for unknown input nonlinear descriptor systems via convex optimization. *IEEE Transactions on Automatic control*, (06), 1047–1052.

Nguyen, M.Q., da Silva, J.G., Sename, O., and Dugard, L. (2015). Semi-active suspension control problem: Some new results using an lpv/h state feedback input constrained control. In *Decision and Control (CDC), 2015 IEEE 54th Annual Conference on*, 863–868. IEEE.

Pertew, A.M., Marquez, H.J., and Zhao, Q. (2006). H/sub/spl infin//observer design for lipschitz nonlinear systems. *IEEE Transactions on Automatic Control*, 51(7), 1211–1216.

Phanomchoeng, G. and Rajamani, R. (2010). Observer design for lipschitz nonlinear systems using riccati equations. In *American Control Conference (ACC), 2010*, 6060–6065. IEEE.

Poussot-Vassal, C., Sename, O., Dugard, L., Gaspar, P., Szabo, Z., and Bokor, J. (2008). A new semi-active suspension control strategy through lpv technique. *Control Engineering Practice*, 16(12), 1519–1534.

Poussot-Vassal, C., Spelta, C., Sename, O., Savaresi, S.M., and Dugard, L. (2012). Survey and performance evaluation on some automotive semi-active suspension control methods: A comparative study on a single-corner model. *Annual Reviews in Control*, 36(1), 148–160.

Priyandoko, G., Mailah, M., and Jamaluddin, H. (2009). Vehicle active suspension system using skyhook adaptive neuro active force control. *Mechanical systems and signal processing*, 23(3), 855–868.

Rajamani, R. (1998). Observers for lipschitz nonlinear systems. *IEEE transactions on Automatic Control*, 43(3), 397–401.

Rajamani, R. and Hedrick, J.K. (1995). Adaptive observers for active automotive suspensions: theory and experiment. *IEEE Transactions on control systems technology*, 3(1), 86–93.

Reichhartinger, M., Falkensteiner, R., and Horn, M. (2018). Robust estimation of forces for suspension system control. In *Joint 9th IFAC Symposium on Robust Control Design and 2nd IFAC Workshop on Linear Parameter Varying Systems*.

Savaresi, S.M., Bittanti, S., and Montiglio, M. (2005). Identification of semi-physical and black-box non-linear models: the case of mr-dampers for vehicles control. *Automatica*, 41(1), 113–127.

Savaresi, S.M., Poussot-Vassal, C., Spelta, C., Sename, O., and Dugard, L. (2010). *Semi-active suspension control design for vehicles*. Elsevier.

Schurter, K.C. and Roschke, P.N. (2000). Fuzzy modeling of a magnetorheological damper using anfis. In *Fuzzy Systems, 2000. FUZZ IEEE 2000. The Ninth IEEE International Conference on*, volume 1, 122–127. IEEE.

Spencer Jr, B., Dyke, S., Sain, M., and Carlson, J. (1997). Phenomenological model for magnetorheological dampers. *Journal of engineering mechanics*, 123(3), 230–238.

Stanway, R., Sproston, J., and Stevens, N. (1987). Nonlinear modelling of an electro-rheological vibration damper. *Journal of Electrostatics*, 20(2), 167–184.

Tudon-Martinez, J.C., Hernandez-Alcantara, D., Sename, O., Morales-Menendez, R., and de J. Lozoya-Santos, J. (2018). Parameter-dependent h filter for lpv semi-active suspension systems. In *Joint 9th IFAC Symposium on Robust Control Design and 2nd IFAC Workshop on Linear Parameter Varying Systems*.

Wen, Y.K. (1976). Method for random vibration of hysteretic systems. *Journal of the engineering mechanics division*, 102(2), 249–263.

Zemouche, A. and Boutayeb, M. (2013). On lmi conditions to design observers for lipschitz nonlinear systems. *Automatica*, 49(2), 585–591.